NUCL SCI TECH (2018) 29:51
https://doi.org/10.1007/s41365-018-0384-2

Transport characteristics of space charge-dominated multi-species deuterium beam in electrostatic low-energy beam line

Xiao-Long Lu[1,2] · Yu Zhang[1,2] · Jun-Run Wang[1,2] · Zhi-Wu Huang[1,3] · Zhan-Wen Ma[1] · Yao Yang[3] · Ze-En Yao[1,2]

Received: 5 May 2017 / Revised: 5 July 2017 / Accepted: 26 July 2017 / Published online: 14 March 2018

Abstract The transport characteristics of a space charge-dominated multi-species deuterium beam consisting of D_1^+, D_2^+, and D_3^+ particles in an electrostatic low-energy beam line are studied. First, the envelope equations of the primary D_1^+ beam are derived considering the space charge effects caused by all particles. Second, the evolution of the envelope of the multi-species deuterium beam is simulated using the PIC code TRACK, with the results showing a significant effect of the unwanted beam on the transport of the primary beam. Finally, different injected beam parameters are used to study beam matching, and a new beam extraction system for the existing duoplasmatron source is designed to obtain the ideal injected beam parameters that allow a D_1^+ beam of up to 50 mA to pass unobstructed through the electrostatic low-energy beam transport line in the presence of an unwanted (D_2^+, D_3^+) beam of 20 mA; at the same time, distortions of the beam emittance and particle distributions are observed.

Keywords Envelope equation · Space charge effects · Multi-species beam · Electrostatic LEBT

This work was supported by the Fundamental Research Funds for the Central Universities (No. lzujbky-2017-93), the National Natural Science Foundation of China (Nos. 11375077, 11027508, and 21327801), and the National Key Scientific Instrument and Equipment Development Projects (No. 2013YQ04086101).

✉ Xiao-Long Lu
luxl@lzu.edu.cn

✉ Ze-En Yao
zeyao@lzu.edu.cn

1 School of Nuclear Science and Technology, Lanzhou University, Lanzhou 730000, China

2 Engineering Research Center for Neutron Application, Ministry of Education, Lanzhou University, Lanzhou 730000, China

3 Institute of Modern Physics, Chinese Academy of Sciences, Lanzhou 730000, China

1 Introduction

High-intensity accelerators such as the high-intensity heavy-ion accelerator facility (HIAF), accelerator-driven sub-critical system (ADS), and intense neutron generator are required for scientific research and industrial applications. High-intensity low-energy beam transport (LEBT) lines are crucial for the development of high-intensity accelerators; however, the associated strong space charge effects present challenges to the transport of high-intensity beams in the LEBTs [1, 2]. The LEBT design is normally based on electrostatic or magnetostatic focusing. The advantage of a magnetostatic LEBT is that the beam can be fully neutralized by the residual gas present in the line, while in an electrostatic LEBT the beam is fully un-neutralized, resulting in strong beam divergence. Therefore, magnetostatic LEBTs are usually adopted. However, electrostatic LEBTs can be very compact because focusing of a high-intensity low-energy beam using an electric field is more effective than using a magnetic field [3]. Hence, electrostatic LEBTs are very attractive for some high-intensity accelerators used in education laboratories and industrial applications, such as high-intensity ion implanters and intense neutron generators based on accelerators [4].

In our laboratory at Lanzhou University, an intense DT/DD neutron generator based on a Cockcroft–Walton accelerator is under construction, and the electrostatic LEBT design is adopted. As shown in Fig. 1, the designed electrostatic LEBT can be viewed as a system of two electrostatic lenses (A1 and A2) combined with a drift tube [5, 6]. The multi-species beam contains D_1^+, D_2^+, and D_3^+ particles directly injected into the electrostatic LEBT; therefore, the transport of the primary particles D_1^+ is affected by the space charge effects not only from the D_1^+ particles themselves but also from the unwanted D_2^+ and D_3^+ particles [7].

In this paper, the envelope equations of the primary beam in an electrostatic LEBT are deduced considering the space charge effects of both the primary and the unwanted beams. In addition, PIC simulations are performed to study the influences of the unwanted beam on the transport of the primary beam. Finally, the influence of the parameters of the beam injected from the duoplasmatron source on the transport of the multi-species beam is studied by the PIC simulations, and a new beam extraction system for the duoplasmatron source is designed.

2 Theoretical analysis

2.1 Beam space charge field

We consider an axisymmetric high-intensity multi-species continuous beam propagating through an axisymmetric electrostatic LEBT. We will use a cylindrical coordinate system (r, z, θ). We consider a uniform charge density profile, which can be expressed as [8]

$$\rho_i(r, s) = \frac{\lambda_i}{\pi r_{\mathrm{b}i}^2(s)}, \tag{1}$$

where λ_i is the linear charge density, $r_{\mathrm{b}i}$ is the beam radius, and $s = z$ is the axial coordinate along the beam direction.

According to Gauss's theorem, $\nabla \cdot E = \frac{\rho}{\varepsilon_0}$, the x-component of the space charge electric field can be expressed as [9]

$$E_{xi}(x) = \begin{cases} \dfrac{I_i}{2\pi\varepsilon_0 \beta_i c r_{\mathrm{b}i}^2} x, & x \le r_{\mathrm{b}i} \\ \dfrac{I_i}{2\pi\varepsilon_0 \beta_i c} \dfrac{x}{r^2}, & x > r_{\mathrm{b}i} \end{cases}, \tag{2}$$

where I_i is the beam current of the species i, $\beta_i c \approx v_{zi}$ is the particle axial velocity in the paraxial approximation, $r = \sqrt{x^2 + y^2}$ is the distance from the beam axis in the radial direction, and x and y are the transverse components in the horizontal and vertical directions, respectively. The constants ε_0, β_i, and c are the permittivity, the relativistic parameter, and the speed of light in vacuum, respectively.

2.2 Envelope equations of a multi-species beam

Assume that the multi-species beam contains particles of two species, a D_1^+ beam with a radius of r_1 and D_2^+ beam with a radius of r_2. The nonrelativistic transverse equation of motion describing a D_1^+ particle evolving in an applied electric accelerating field and the beam space charge field can be written as [10]

$$m_1 \ddot{x} = q\left(E_x^{\mathrm{appl}} + E_{D_1 x}^{\mathrm{self}} + E_{D_2 x}^{\mathrm{self}}\right), \tag{3}$$

Here, $\ddot{x} = v_{z1}^2 x'' + v_{z1} v_{z1}' x'$; primes denote derivatives with respect to the axial coordinate z; $v_{z1} \approx \beta_1 c$ is the axial velocity of the D_1^+ particle; m_1 and q are the mass and charge of the D_1^+ particle, respectively; E_x^{appl}, $E_{D_1 x}^{\mathrm{self}}$, and

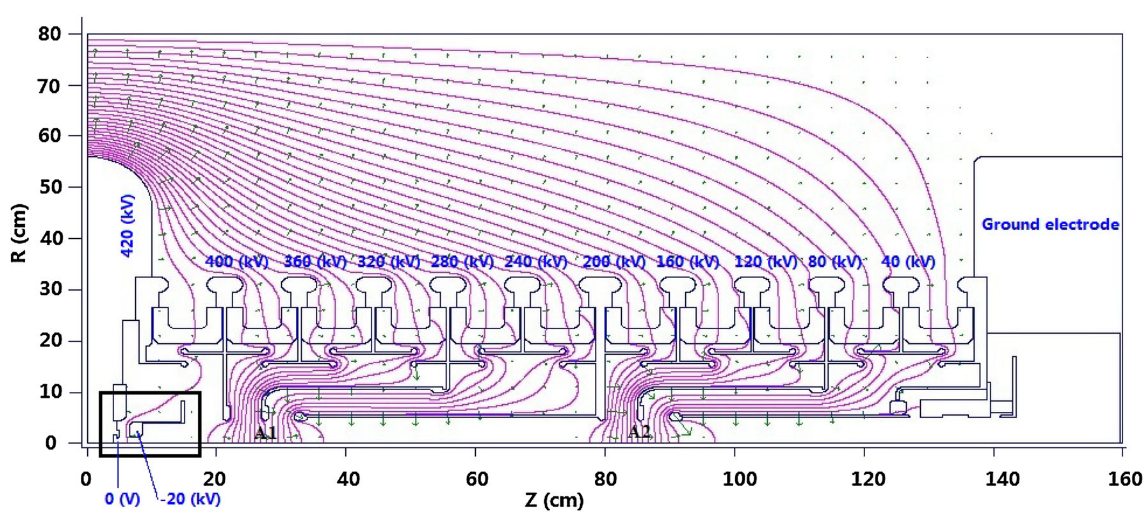

Fig. 1 (Color online) Electrostatic LEBT for a multi-species deuterium beam; the beam extraction system of the duoplasmatron source is indicated by the black rectangle; the voltage values are shown; the pink lines represent equipotential surfaces

$E_{D_2x}^{\rm self}$ are the applied electric field, the space charge field of the D_1^+ beam, and the space charge field of the D_2^+ beam along the x-direction, respectively.

In the paraxial approximation, $E_x^{\rm appl}=-\frac{1}{2}\frac{\partial^2\varphi}{\partial z^2}x=-\frac{\varphi''}{2}x$, φ is the normalized potential corresponding to the applied on-axis electric field, $q\varphi=\frac{1}{2}m_1\beta_1^2c^2$, while $E_{D_1x}^{\rm self}$ and $E_{D_2x}^{\rm self}$ can be calculated with Eq. (2). Then, the equations of motion of the D_1^+ particle in the x-direction can be written as [11]

$$\begin{cases} x''+\dfrac{\varphi'}{2\varphi}x'+\dfrac{\varphi''}{4\varphi}x-\dfrac{I_1}{4\varphi\pi\varepsilon_0\beta_1cr_1^2}x-\dfrac{I_2}{4\varphi\pi\varepsilon_0\beta_2cr_2^2}x=0 & (r_1\le r_2)\\ x''+\dfrac{\varphi'}{2\varphi}x'+\dfrac{\varphi''}{4\varphi}x-\dfrac{I_1}{4\varphi\pi\varepsilon_0\beta_1c}\dfrac{x}{r_1^2}-\dfrac{I_2}{4\varphi\pi\varepsilon_0\beta_2c}\dfrac{x}{r^2}=0 & (r_1>r_2)\end{cases}. \tag{4}$$

In order to derive the envelope equations, we let $R_x^2=X_{\rm b}^2=2\langle x^2\rangle$, where $X_{\rm b}$ is the beam envelope in the x-direction, and $\langle x^2\rangle=\frac{\int_0^{r_{\rm bi}}\int_0^{2\pi}x^2\rho(r,s)r{\rm d}r{\rm d}\theta}{\int_0^{r_{\rm bi}}\int_0^{2\pi}\rho(r,s)r{\rm d}r{\rm d}\theta}$ is the transverse average of the particles [8–11]. Then,

$$X_{\rm b}''=\frac{2\langle xx''\rangle}{X_{\rm b}}+\frac{4\langle x^2\rangle\langle x'^2\rangle-4\langle xx'\rangle^2}{X_{\rm b}^3}, \tag{5}$$

For $r_1\le r_2$, Eq. (4) can be transformed into Eq. (6) by multiplying by x and averaging over the distribution of the particles,

$$\langle xx''\rangle+\frac{\varphi'}{2\varphi}\langle xx'\rangle+\frac{\varphi''}{4\varphi}\langle x^2\rangle-\frac{I_1}{4\varphi\pi\varepsilon_0\beta_1cr_1^2}\langle x^2\rangle-\frac{I_2}{4\varphi\pi\varepsilon_0\beta_2cr_2^2}\langle x^2\rangle=0, \tag{6}$$

Thus, combining Eq. (5) with Eq. (6), the envelope for the D_1^+ species of the multi-species beam can be described as

$$X_{\rm b}''+\frac{\phi'}{2\phi}X_{\rm b}'+\frac{\phi''}{4\phi}X_{\rm b}-\frac{I_1}{4\phi\pi\varepsilon_0\beta_1c}\frac{1}{X_{\rm b}}-\frac{I_2}{4\phi\pi\varepsilon_0\beta_2c}\frac{1}{X_{\rm bd2}^2}X_{\rm b}-\frac{\varepsilon_{\rm xd1}^2}{X_{\rm b}^3}=0, \tag{7}$$

where $X_{\rm bd2}$ is the beam envelope of the D_2^+ species in the x-direction, ε_{xd1} is the beam emittance of the D_1^+ species in the x-direction, and

$$\varepsilon_{\rm xd1}^2=4\langle x^2\rangle\langle x'^2\rangle-4\langle xx'\rangle^2.$$

Similarly, for $r_1>r_2$, Eq. (5) can be written as

$$\langle xx''\rangle+\frac{\phi'}{2\phi}\langle xx'\rangle+\frac{\phi''}{4\phi}\langle x^2\rangle-\frac{I_1}{4\phi\pi\varepsilon_0\beta_1c}\frac{1}{r_1^2}\langle x^2\rangle-\frac{I_2}{4\phi\pi\varepsilon_0\beta_2c}\left\langle\frac{x^2}{r^2}\right\rangle=0, \tag{8}$$

where
$$\left\langle\frac{x^2}{r^2}\right\rangle=\frac{\int_{r_2}^{r_1}\int_0^{2\pi}\frac{x^2}{r^2}\rho_1(r,s)r{\rm d}r{\rm d}\theta}{\int_0^{r_1}\int_0^{2\pi}\rho_1(r,s)r{\rm d}r{\rm d}\theta}=\frac{1}{2}\left(1-\frac{r_2^2}{r_1^2}\right)=\frac{1}{2}\left(1-\frac{X_{\rm bd2}^2}{X_{\rm b}^2}\right), \tag{9}$$

Thus, the envelope for the D_1^+ species of the multi-species beam can be described as

$$X_{\rm b}''+\frac{\phi'}{2\phi}X_{\rm b}'+\frac{\phi''}{4\phi}X_{\rm b}-\frac{I_1}{4\phi\pi\varepsilon_0\beta_1c}\frac{1}{X_{\rm b}}-\frac{I_2}{4\phi\pi\varepsilon_0\beta_2c}\frac{1}{2}\left(1-\frac{X_{\rm bd2}^2}{X_{\rm b}^2}\right)-\frac{\varepsilon_{\rm xd1}^2}{X_{\rm b}^3}=0, \tag{10}$$

From the above, the x-direction envelope for the D_1^+ species of the multi-species beam consisting of D_1^+ and D_2^+ can be expressed as

$$\begin{cases} X_{\rm b}''+\dfrac{\phi'}{2\phi}X_{\rm b}'+\dfrac{\phi''}{4\phi}X_{\rm b}-\dfrac{I_1}{4\phi\pi\varepsilon_0\beta_1c}\dfrac{1}{X_{\rm b}}-\dfrac{I_2}{4\phi\pi\varepsilon_0\beta_2c}\dfrac{1}{X_{\rm bd2}^2}X_{\rm b}-\dfrac{\varepsilon_{\rm xd1}^2}{X_{\rm b}^3}=0 & (r_1\le r_2)\\ X_{\rm b}''+\dfrac{\phi'}{2\phi}X_{\rm b}'+\dfrac{\phi''}{4\phi}X_{\rm b}-\dfrac{I_1}{4\phi\pi\varepsilon_0\beta_1c}\dfrac{1}{X_{\rm b}}-\dfrac{I_2}{4\phi\pi\varepsilon_0\beta_2c}\dfrac{1}{2}\left(1-\dfrac{X_{\rm bd2}^2}{X_{\rm b}^2}\right)-\dfrac{\varepsilon_{\rm xd1}^2}{X_{\rm b}^3}=0 & (r_1>r_2)\end{cases}, \tag{11}$$

In the y-direction, the envelope equations have a similar form.

For the multi-species beam containing D_1^+, D_2^+, and D_3^+, Eq. (3) can be written as

$$m_1\ddot{x} = q\left(E_x^{\mathrm{appl}} + E_{D_1x}^{\mathrm{self}} + E_{D_2x}^{\mathrm{self}} + E_{D_3x}^{\mathrm{self}}\right), \tag{12}$$

where $E_{D_3x}^{\mathrm{self}}$ is the space charge field of the D_3^+ beam along the x-direction.

Then, the equations of motion of D_1^+ in x-direction can be described as

$$\begin{cases} x'' + \dfrac{\phi'}{2\phi}x' + \dfrac{\phi''}{4\phi}x - \dfrac{I_1}{4\phi\pi\varepsilon_0\beta_1 c r_1^2}x - \dfrac{I_2}{4\phi\pi\varepsilon_0\beta_2 c r_2^2}x - \dfrac{I_3}{4\phi\pi\varepsilon_0\beta_3 c r_3^2}x = 0 & (r_1 \le r_2, r_1 \le r_3) \\ x'' + \dfrac{\phi'}{2\phi}x' + \dfrac{\phi''}{4\phi}x - \dfrac{I_1}{4\phi\pi\varepsilon_0\beta_1 c}\dfrac{x}{r_1^2} - \dfrac{I_2}{4\phi\pi\varepsilon_0\beta_2 c}\dfrac{x}{r^2} - \dfrac{I_3}{4\phi\pi\varepsilon_0\beta_3 c}\dfrac{x}{r^2} = 0 & (r_1 > r_2, r_1 > r_3) \\ x'' + \dfrac{\phi'}{2\phi}x' + \dfrac{\phi''}{4\phi}x - \dfrac{I_1}{4\phi\pi\varepsilon_0\beta_1 c r_1^2}x - \dfrac{I_2}{4\phi\pi\varepsilon_0\beta_2 c r_2^2}x - \dfrac{I_3}{4\phi\pi\varepsilon_0\beta_3 c}\dfrac{x}{r^2} = 0 & (r_3 < r_1 \le r_2) \\ x'' + \dfrac{\phi'}{2\phi}x' + \dfrac{\phi''}{4\phi}x - \dfrac{I_1}{4\phi\pi\varepsilon_0\beta_1 c}\dfrac{x}{r_1^2} - \dfrac{I_2}{4\phi\pi\varepsilon_0\beta_2 c}\dfrac{x}{r^2} - \dfrac{I_3}{4\phi\pi\varepsilon_0\beta_3 c r_3^2}x = 0 & (r_2 < r_1 \le r_3) \end{cases}, \tag{13}$$

Using the same method as that used for the derivation of Eq. (11), the x-direction envelope for the D_1^+ species of the multi-species beam consisting of D_1^+, D_2^+, and D_3^+ can be expressed as

$$\begin{cases} X''_{\mathrm{b}} + \dfrac{\phi'}{2\phi}X'_{\mathrm{b}} + \dfrac{\phi''}{4\phi}X_{\mathrm{b}} - \dfrac{I_1}{4\phi\pi\varepsilon_0\beta_1 c}\dfrac{1}{X_{\mathrm{b}}} - \dfrac{I_2}{4\phi\pi\varepsilon_0\beta_2 c}\dfrac{1}{X_{\mathrm{bd2}}^2}X_{\mathrm{b}} - \dfrac{I_3}{4\phi\pi\varepsilon_0\beta_3 c}\dfrac{1}{X_{\mathrm{bd3}}^2}X_{\mathrm{b}} - \dfrac{\varepsilon_{x\mathrm{d1}}^2}{X_{\mathrm{b}}^3} = 0 & (r_1 \le r_2, r_1 \le r_3) \\ X''_{\mathrm{b}} + \dfrac{\phi'}{2\phi}X'_{\mathrm{b}} + \dfrac{\phi''}{4\phi}X_{\mathrm{b}} - \dfrac{I_1}{4\phi\pi\varepsilon_0\beta_1 c}\dfrac{1}{X_{\mathrm{b}}} - \dfrac{I_2}{4\phi\pi\varepsilon_0\beta_2 c}\dfrac{1}{2}\left(1 - \dfrac{X_{\mathrm{bd2}}^2}{X_b^2}\right) - \dfrac{I_3}{4\phi\pi\varepsilon_0\beta_3 c}\dfrac{1}{2}\left(1 - \dfrac{X_{\mathrm{bd3}}^2}{X_b^2}\right) - \dfrac{\varepsilon_{x\mathrm{d1}}^2}{X_{\mathrm{b}}^3} = 0 & (r_1 > r_2, r_1 > r_3) \\ X''_{\mathrm{b}} + \dfrac{\phi'}{2\phi}X'_{\mathrm{b}} + \dfrac{\phi''}{4\phi}X_{\mathrm{b}} - \dfrac{I_1}{4\phi\pi\varepsilon_0\beta_1 c}\dfrac{1}{X_{\mathrm{b}}} - \dfrac{I_2}{4\phi\pi\varepsilon_0\beta_2 c}\dfrac{1}{X_{\mathrm{bd2}}^2}X_{\mathrm{b}} - \dfrac{I_3}{4\phi\pi\varepsilon_0\beta_3 c}\dfrac{1}{2}\left(1 - \dfrac{X_{\mathrm{bd3}}^2}{X_{\mathrm{b}}^2}\right) - \dfrac{\varepsilon_{x\mathrm{d1}}^2}{X_b^3} = 0 & (r_3 < r_1 \le r_2) \\ X''_{\mathrm{b}} + \dfrac{\phi'}{2\phi}X'_{\mathrm{b}} + \dfrac{\phi''}{4\phi}X_{\mathrm{b}} - \dfrac{I_1}{4\phi\pi\varepsilon_0\beta_1 c}\dfrac{1}{X_{\mathrm{b}}} - \dfrac{I_2}{4\phi\pi\varepsilon_0\beta_2 c}\dfrac{1}{2}\left(1 - \dfrac{X_{\mathrm{bd2}}^2}{X_{\mathrm{b}}^2}\right) - \dfrac{I_3}{4\phi\pi\varepsilon_0\beta_3 c}\dfrac{1}{X_{\mathrm{bd3}}^2}X_{\mathrm{b}} - \dfrac{\varepsilon_{x\mathrm{d1}}^2}{X_{\mathrm{b}}^3} = 0 & (r_2 < r_1 \le r_3) \end{cases}, \tag{14}$$

In the y-direction, the envelope equations for the particles of the three species have a similar form.

3 Simulation

3.1 Beam extraction system of the duoplasmatron source

3.1.1 Current operational beam extraction system

The current operational duoplasmatron ion source has been used for decades, and it is very reliable. The particle distributions in the phase space obtained in previous experiments [12] are shown in Fig. 2. For the LEBT simulation, the following parameters of the old beam extraction system are assumed [5]: The normalized beam emittance is $\varepsilon_x = \varepsilon_y = 0.71$ mm mrad, and the Twiss parameters are $\alpha_x = \alpha_y = -4$ and $\beta_x = \beta_y = 80$ cm/rad, respectively. The fraction of D_1^+ in the multi-species beam is approximately 75%, and D_2^+ and D_3^+ comprise approximately 18% and approximately 7% of the total beam, respectively.

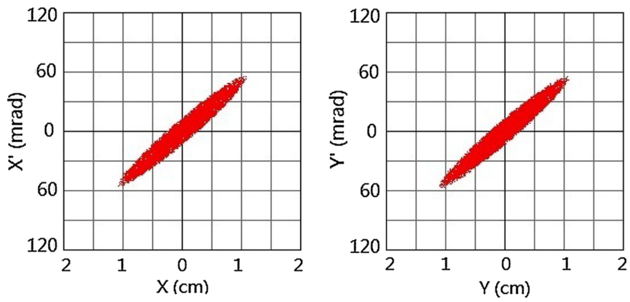

Fig. 2 (Color online) Particle distributions in the phase space for the old beam extraction system [12]

3.1.2 *New designed beam extraction system*

As shown in Fig. 3, a new beam extraction system of the duoplasmatron source is designed by the PIC simulation method [13]. Compared to the old beam extraction system, the size of the extraction electrode, the dip angle of the anode, and the distance between the anode and the extraction electrode are changed. In addition, two small permanent magnet lenses with a magnetic strength of 1000 Gs are added. The simulated particle distributions in the phase space are shown in Fig. 4, where the normalized beam emittance is $\varepsilon_x = \varepsilon_y = 2.5$ mm mrad, and the Twiss parameters are $\alpha_x = \alpha_y = -3.5$ and $\beta_x = \beta_y = 57$ cm/rad, respectively.

3.2 Transport characteristics of the multi-species beam

3.2.1 *Effects of the unwanted beam composition on the primary beam transport*

It is clear that using a pure beam is beneficial for improving the beam transport efficiency and decreasing the beam power. Therefore, various beam separation elements, such as dipole-bending magnets, Wien filters, or apertures combined with solenoids, are usually utilized to obtain a pure beam in the LEBT [3]. However, using such beam separation elements will not only have the disadvantage of significantly increasing the length of the LEBT but is also not conducive to industrial application marketing due to the increased cost. In our scheme, the multi-species beam will be injected into the electrostatic LEBT directly.

In order to understand the influence of the unwanted beam on the primary beam, the evolution of the D^+ beam envelope for various ratios of species in the multi-species beam is simulated using the PIC code TRACK [14]. The simulation results are illustrated in Fig. 5. They show that the envelope radius of the D_1^+ beam increases with the increasing unwanted beam intensity. The four envelopes corresponding to Beam (40 mA D_1^+), Beam (30 mA D_1^+, 10 mA D_2^+), Beam (30 mA D_1^+, 10 mA D_3^+), and Beam (30 mA D_1^+, 5 mA D_2^+, 5 mA D_3^+) almost fully overlap. The two envelopes corresponding to Beam (30 mA D_1^+, 5 mA D_2^+) and Beam (30 mA D_1^+, 5 mA D_3^+) almost fully overlap as well. This illustrates that the total intensity of the unwanted beams has a significant influence on the primary beam divergence. However, the influence of each species on the primary beam envelope is not obvious.

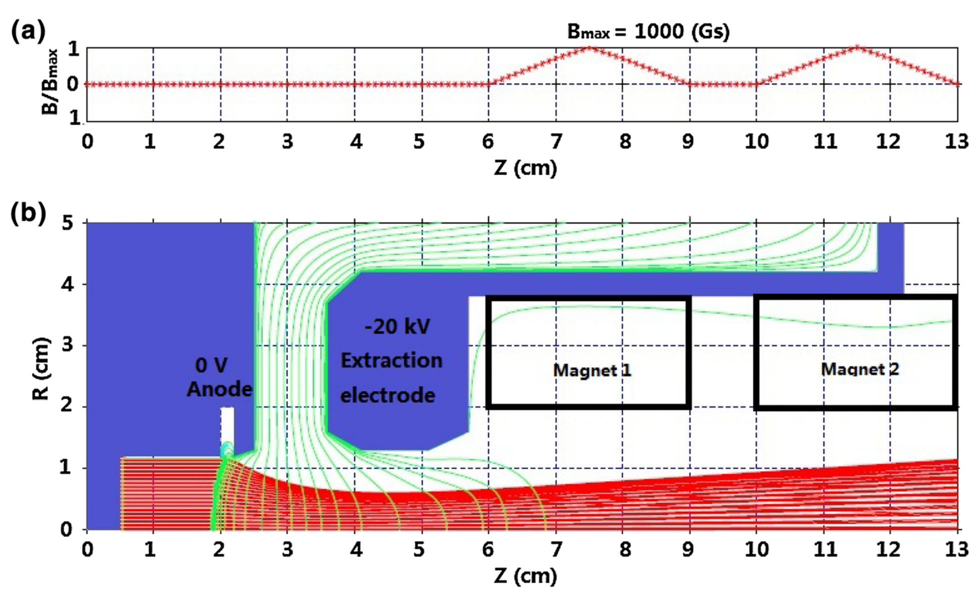

Fig. 3 (Color online) New designed beam extraction system: **a** axial magnetic field; **b** configuration of the system, where the red lines represent the trajectories of the 50 mA D_1^+ beam, and the green lines represent equipotential surfaces

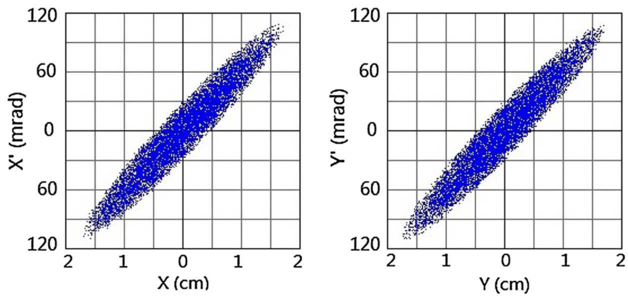

Fig. 4 (Color online) Particle distributions in the phase space for the new designed beam extraction system

3.2.2 Effects of the injection beam parameters on the multi-species beam transport

Matching the extracted beam to the subsequent electrostatic LEBT beam is important for high-intensity beam transport [15]. Therefore, two different sets of the injected beam parameters from the old beam extraction system and the new designed beam extraction system, as described above, are used to simulate the effects of these parameters on the transport of the multi-species beam by the PIC code TRACK. The results are described below.

3.2.2.1 Transport efficiency For the LEBT simulation, we use two different sets of the initial beam parameters obtained from the new and old beam extraction systems. For the new beam extraction system, the beam envelope radius is $X_{D1} = X_{D2} = X_{D3} = 1.7$ cm, and the beam divergence angle is $X'_{D1} = X'_{D2} = X'_{D3} = 110$ mrad. For the old beam extraction system, the beam envelope radius is $X_{D1} = X_{D2} = X_{D3} = 1.1$ cm, and the beam divergence angle is $X'_{D1} = X'_{D2} = X'_{D3} = 55$ mrad. The intensity of each species and the simulation results are shown in Fig. 6. It can be seen that using the initial beam parameters obtained from the new beam extraction system reduces the beam divergence for the beam transport in the electrostatic LEBT.

The beam transport efficiency of each species in the electrostatic LEBT is simulated by the PIC code. The intensities of the D_1^+, D_2^+, and D_3^+ beams are 50, 10, and 10 mA, respectively. The beam envelope radius and divergence angle are the same with those described in the previous paragraph. The simulation results are shown in Fig. 7. When the initial beam parameters obtained from the new extraction system are used for the simulation, the transport efficiency of the D_1^+, D_2^+, and D_3^+ beams are 100, 94, and 39%, respectively. For the old beam extraction system, the corresponding values are 100, 58, and 52%. This implies that in the new beam extraction system, the D_3^+ beam will quickly hit the LEBT pipe and lose the majority of its particles.

3.2.2.2 Emittance distortion and particle distributions In the electrostatic LEBT, due to the presence of high electrostatic fields, the high-intensity beam is fully un-neutralized. The space charge effect of the un-neutralized beam will cause a significant increase in emittance and strong beam filamentation. In addition, the nonlinear space charge field will cause emittance distortion [16]. At the same time, the beam parameters at the output of the electrostatic LEBT are important for matching the beam to the subsequent beam transport elements. Therefore, we simulate the beam emittance and particle distributions. In the

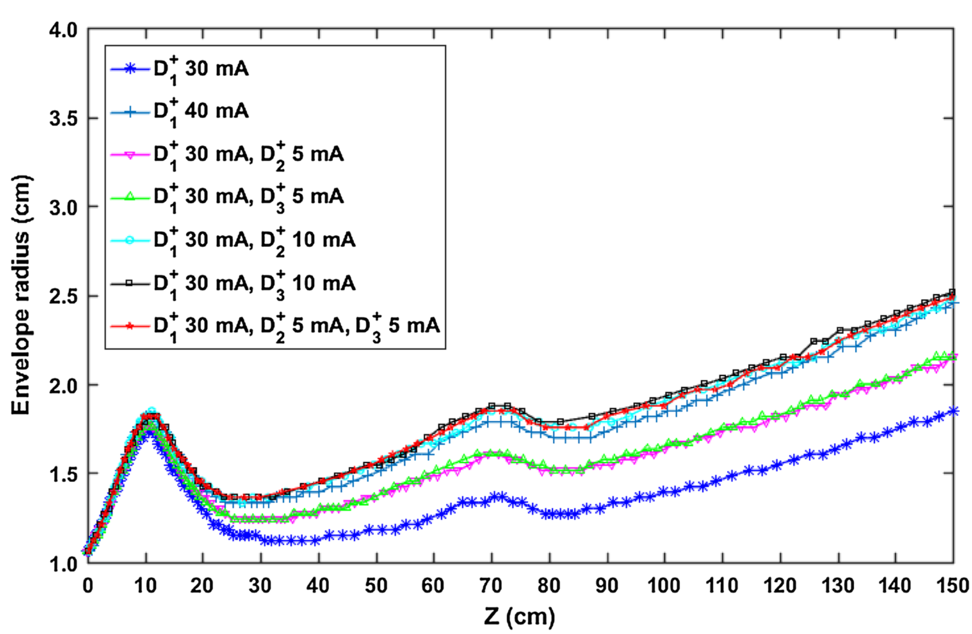

Fig. 5 (Color online) Evolution of the D_1^+ beam envelopes of the multi-species beam with different ratios of the species

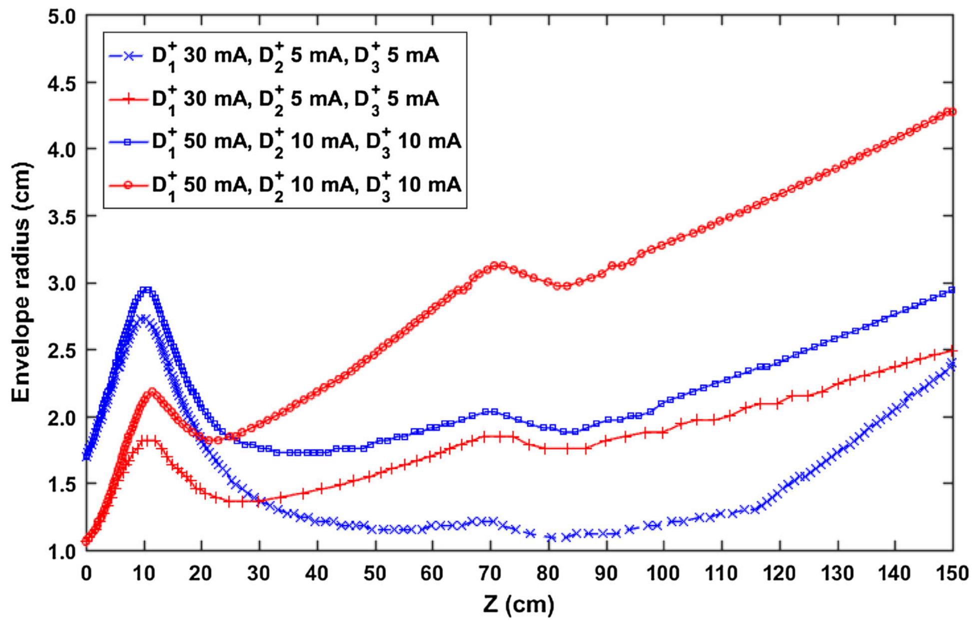

Fig. 6 (Color online) Evolution of the D_1^+ beam envelopes of the multi-species beam with different ratios of the species for different injected beam parameters

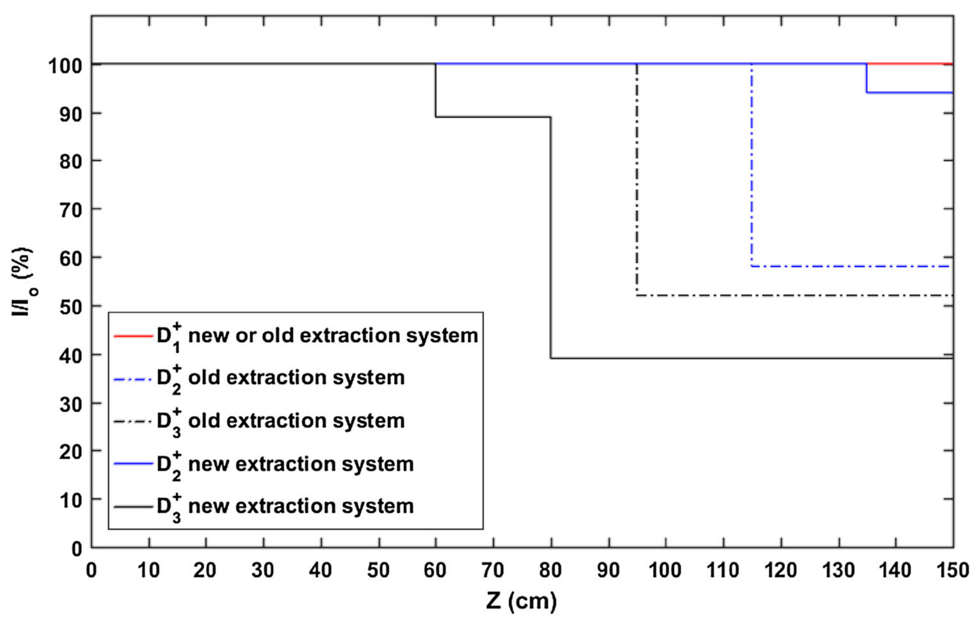

Fig. 7 (Color online) Transport efficiency of each species beam for the new and old beam extraction systems

simulation, the fraction of each species beam is set based on the current operational duoplasmatron source, and the intensities of the D_1^+, D_2^+, and D_3^+ beams are set to 30, 7, and 3 mA, respectively. For the new beam extraction system, the beam envelope radius is $X_{D1} = X_{D2} = X_{D3} = 1.7$ cm, and the beam divergence angle is $X'_{D1} = X'_{D2} = X'_{D3} = 110$ mrad. For the old beam extraction system, the beam envelope radius is $X_{D1} = X_{D2} = X_{D3} = 1.1$ cm, and the beam divergence angle is $X'_{D1} = X'_{D2} = X'_{D3} = 55$ mrad. A water-bag distribution is used. The simulation results are shown in Figs. 8, 9 and 10.

Figure 8 shows the simulated envelopes of the multi-species beam with different injected beam parameters, confirming that the injected beam parameters have a significant influence on the transport of the multi-species beam, and therefore, it is necessary to match the beam to the electrostatic LEBT by optimizing the injected beam parameters.

Figure 9 shows the simulated beam emittance at the output of the electrostatic LEBT for different injected beam parameters. It can be seen that, for the new designed beam extraction system (Fig. 9a, b), the emittance distortion of the primary D_1^+ beam at the output of the electrostatic

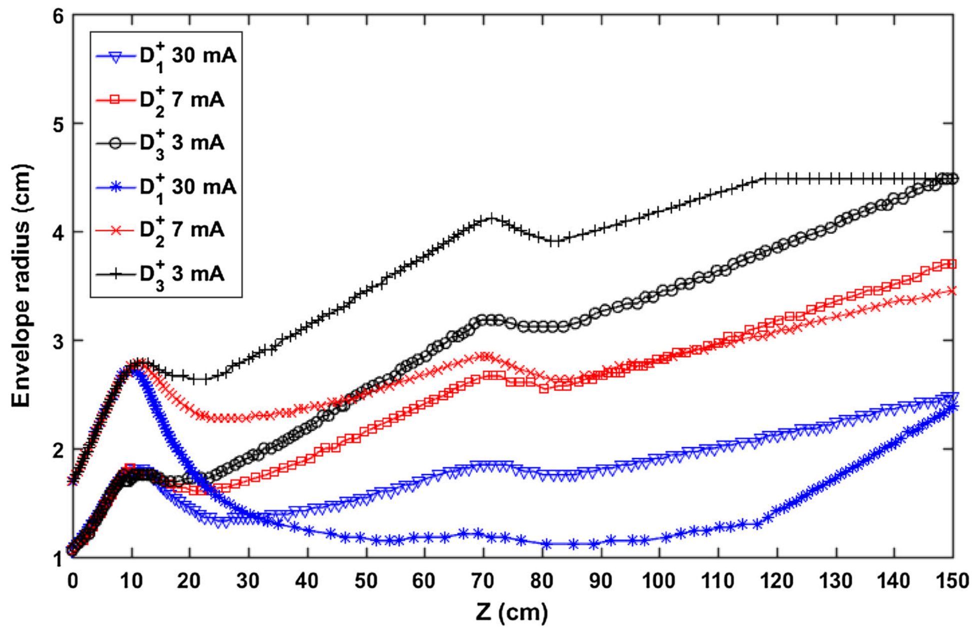

Fig. 8 (Color online) Evolution of the envelopes of the multi-species beam for different injected beam parameters

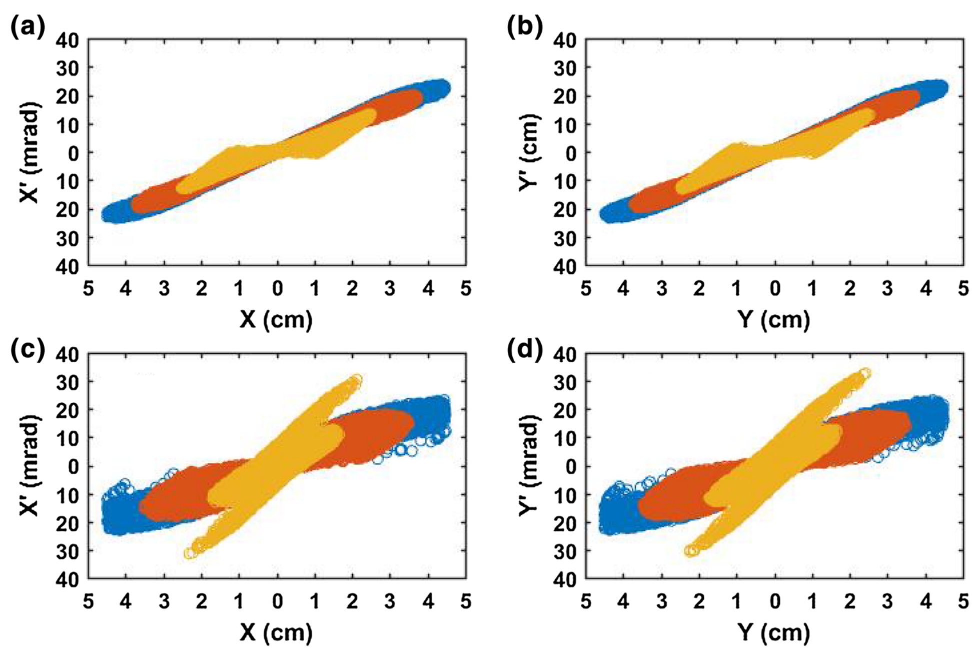

Fig. 9 (Color online) Beam emittance at the output of the electrostatic LEBT; D_1^+, D_2^+, and D_3^+ are represented by yellow, orange, and blue points, respectively; particle x–x' (**a**) and particle y–y' (**b**) with the injected beam parameters for the old beam extraction system; particle x–x' (**c**) and particle y–y' (**d**) with the injected beam parameters for the new designed beam extraction system

LEBT is more severe than that for the old beam extraction system (Fig. 9c, d); however, the particle distributions of the primary beam are more focused, as shown in Fig. 10. For the new designed beam extraction system, the emittance of the primary beam at the output is approximately 10.1 mm mrad, $\sim$ 4 times greater than that at the input, which is approximately 2.5 mm mrad. However, for the old beam extraction system, the emittance of the primary beam at the output is approximately 9.1 mm mrad, $\sim$ 12 times greater than that at the input, which is approximately 0.7 mm mrad.

Figure 10 shows that hollow beams are formed for all species (D_1^+, D_2^+, and D_3^+) when the beam is extracted from the old beam extraction system. From Fig. 10a, the hollow structure of the D_1^+ beam is obvious, and exhibits a spot size of approximately 5 cm. However, in Fig. 10b, this effect is reduced significantly, and the spot size of the beam for the new extraction system is approximately 3 cm, which is obtained considering 98% of all D_1^+ particles and neglecting the distorted portion. It is found that the appropriate injected beam parameters play an important role in both the beam transport and the beam spot size in

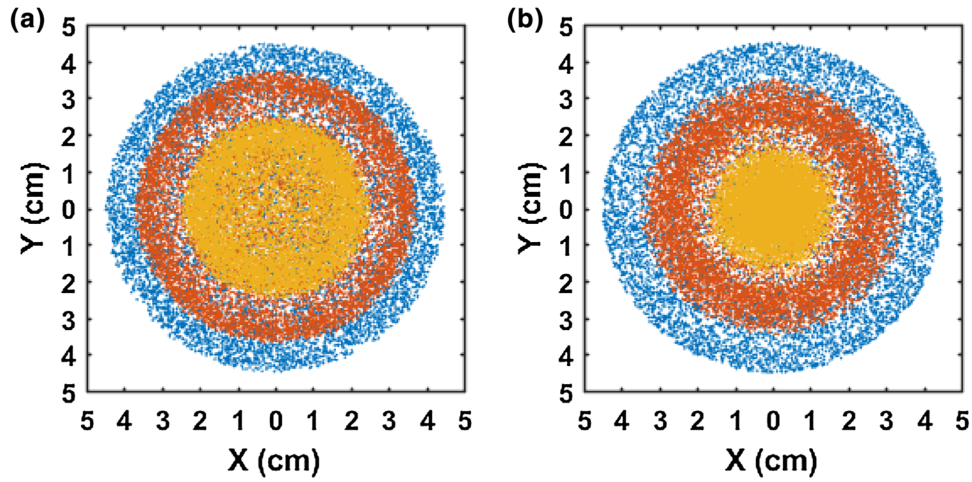

Fig. 10 (Color online) Particle distributions in real space at the output of the electrostatic LEBT; D_1^+, D_2^+, and D_3^+ are represented by yellow, orange, and blue points, respectively; of the two graphs correspond to the old (**a**) and new designed (**b**) beam extraction systems, respectively

the electrostatic LEBT. This can be helpful for developing compact ion implanters and intense neutron generators.

4 Conclusion

The envelope equations of the multi-species deuterium beam in an electrostatic LEBT are derived considering the space charge effects caused by the particles of all species. The evolution of the envelopes of the multi-species beam is simulated in the presence of different ratios of the components D_1^+, D_2^+, and D_3^+, and for two sets of the injected beam parameters corresponding to the old and new beam extraction systems of the duoplasmatron source. The simulation results show that the envelope radius of the D_1^+ beam increases with the increase in the unwanted beam intensity. The new injected beam parameters improve the transport of the primary beam in the electrostatic LEBT. However, the corresponding emittance is found to be distorted at the output of the electrostatic LEBT. The results indicate that, with the appropriate injected beam parameters, an electrostatic LEBT is a promising choice for developing compact ion implanters and intense neutron generators.

References

1. N. Chauvin, O. Delferrière, R. Duperrier et al., Transport of intense ion beams and space charge compensation issues in low energy beam lines. Rev. Sci. Instrum. **83**, 02B320 (2012). https://doi.org/10.1063/1.3678658
2. P. Sing Babu, A. Goswami, V.S. Pandit, Transport of intense proton beam in the presence of subdominant species in a low energy beam transport system. J. Instrum. **11**, P04020 (2016). https://doi.org/10.1088/1748-0221/11/04/P04020
3. Y.K. Batygin, I.N. Draganic, C.M. Fortgang et al., Design of low energy beam transport for new LANSCE H + injector. Nucl. Instrum. Methods A **753**, 1 (2014). https://doi.org/10.1016/j.nima.2014.03.041
4. I.S. Anderson, C. Andreani, J.M. Carpenter et al., Research opportunities with compact accelerator-driven neutron sources. Phys. Rep. **654**, 1 (2016). https://doi.org/10.1016/j.physrep.2016.07.007
5. X.L. Lu, J.R. Wang, Y. Zhang et al., Design of a high-current low-energy beam transport line for an intense DT/DD neutron generator. Nucl. Instrum. Methods A **811**, 76 (2016). https://doi.org/10.1016/j.nima.2015.11.156
6. X.L. Lu, Z.E. Yao, Y. Zhang et al., Simulation of high-intense beam transport in electrostatic accelerating column. Nucl. Sci. Tech. **26**, 060201 (2015). https://doi.org/10.13538/j.1001-8042/nst.26.060201
7. P. Sing Babu, A. Goswami, V.S. Pandit, Effect of subdominant species on the evolution of intense primary beam in a low energy beam transport line. Phys. Plasmas **20**, 083110 (2013). https://doi.org/10.1063/1.4817952
8. S. Lund, J. Barnard, US Particle Accelerator School, Beam Physics with Intense Space Charge. (2015). https://people.nscl.msu.edu/~lund/uspas/bpisc_2015/. Accessed 10 Sep 2016
9. P. Sing Babu, A. Goswami, V.S. Pandit, Envelope equations for cylindrically symmetric space charge dominated multi species beam. Phys. Plasmas **18**, 103117 (2011). https://doi.org/10.1063/1.3651200
10. G.J. Zhao, B.J. Ling, K.X. Xue, *Optics of ions and electrons* (National Defense Industry Press, Beijing, 1994). **(in Chinese)**
11. M. Reiser, *Theory and design of charge particle beams* (Wiley Press, New York, 2008)
12. B.H. Sun, Q. Chen, Characteristics of intense beam for a duoplasmatron source. Nucl. Tech. **14**, 731 (1991). **(in Chinese)**
13. O. Sutherland, J. Keller, M. Irzyk et al., Comparison between experiment and two simulation strategies for the extraction of focused ion beams. Rev. Sci. Instrum. **75**, 2379 (2004). https://doi.org/10.1063/1.1753669
14. P.N. Ostroumov, User manual. http://www.phy.anl.gov/atlas/TRACK/. Accessed 16 March 2016
15. V.W. Krauss, H. Beuscher, H.L. Hagedoorn et al., Emittance and matching of ECR sources. Nucl. Instrum. Methods A **268**, 5 (1988). https://doi.org/10.1016/0168-9002(88)90586-4
16. Y.K. Batygin, Conservation of space-charge-dominated beam emittance in a strong nonlinear focusing field. Phys. Rev. E **53**, 5358 (1996). https://doi.org/10.1103/PhysRevE.53.5358